Characterization of ω-Functionalized Undecanethiol Mixed Self-Assembled Monolayers on Au(111): A Combined Polarization Modulation Infrared Reflection – Absorption Spectroscopy/X-ra...

ARTICLE *in* THE JOURNAL OF PHYSICAL CHEMISTRY C · JANUARY 2008

Impact Factor: 4.77 · DOI: 10.1021/jp074023c

4 AUTHORS:

Frederik Tielens
Collège de France
93 PUBLICATIONS **1,330** CITATIONS
SEE PROFILE

Dominique Costa
MINES ParisTech
94 PUBLICATIONS **1,770** CITATIONS
SEE PROFILE

Vincent Humblot
Pierre and Marie Curie University - Paris 6
57 PUBLICATIONS **1,336** CITATIONS
SEE PROFILE

Claire-Marie Pradier
Pierre and Marie Curie University - Paris 6
170 PUBLICATIONS **2,830** CITATIONS
SEE PROFILE

Characterization of ω-Functionalized Undecanethiol Mixed Self-Assembled Monolayers on Au(111): A Combined Polarization Modulation Infrared Reflection−Absorption Spectroscopy/X-ray Photoelectron Spectroscopy/Periodic Density Functional Theory Study

Frederik Tielens,* Dominique Costa, Vincent Humblot, and Claire-Marie Pradier

Laboratoire de Réactivité de Surface, Université Pierre et Marie Curie-Paris6, UMR 7609, Tour 54-55, 2ème étage - Casier 178, 4, Place Jussieu, F-75252 Paris Cedex 05, France

Received: May 24, 2007; In Final Form: August 30, 2007

The structure of undecanethiol self-assembled monolayers (SAMs) on Au(111) with −COOH and −OH tail groups has been characterized by combining experimental and theoretical techniques. The pure and mixed 1:1 SAMs were investigated. It was found using polarization modulation infrared reflection−absorption spectroscopy, X-ray photoelectron spectroscopy (XPS), and ab initio calculation methods that the chains adsorb via their S atom on two different sites (one near atop and another near bridge site) of the Au(111) surface and that inter-tail-group H bonds are formed, leading to chain paring. Only some traces of aggregation between the different chain types were observed, confirming our former atomic force microscopy results. The vibrational frequencies and XPS results obtained via both experimental and theoretical approaches have enabled to describe and understand the adsorbed mixed and pure thiol SAMs.

Introduction

Immersion of a gold surface in thiolate solution leads to a spontaneous adsorption of thiols.[1] These types of layers have attracted much attention because they may constitute ideal platforms for further binding or reactivity. Thiolate rapidly adsorb to form a quasisaturated layer in a few minutes to an hour; this preliminary adsorption step is followed by an ordering of the thiolate chains leading to a crystalline-like layer depending on time and conditions of immersion. Some authors claim that 1 day or more are necessary to reach the equilibrium between the surface and the solution.[2−4]

Alkanethiolate layers on Au(111) lead to densely packed ($\sqrt{3} \times \sqrt{3}$)*R*30° structures that have been well characterized using different experimental techniques as well as theoretical calculations; the main results are summarized in recent reviews.[5,6] It was concluded in these reviews that we have now a general description of the surface structure, hence with still some controversial points. One of these points is, e.g., the adsorption sites on the substrates preferred by the thiol adsorption.

The influence of the chain lengths and of the nature of the tail groups on the SAM structure are two factors which have found a wide interest. The authors now agree on the number of CH_2 groups, being 10, from which adsorbed thiols spontaneously form densely packed ordered all gauge layers.[7−9]

The second factor, however, has been less studied despite the interest of building surfaces with well-controlled functionality[10] such as for the binding of proteins.[11,12] Allara et al. characterized a series of polyfunctional organic monolayers; they concluded that changing the tail group has little effect on the film structure but that the functional groups adopt specific orientations suggesting important intergroup interactions.[13] COOH-terminated self-assembled monolayers (SAMs) were clearly shown to exhibit intermolecular interactions, likely hydrogen binding, as revealed by small intermolecular distances.[14] Intermolecular interactions were even stronger, facilitated by H bonding, when the layers were rinsed in aqueous solution.[15]

In the frame of elaborating adjusted surface functionalities for biocompatibility, biosensor, or molecular electronics, special effort was made to form two-component monolayers, in order to avoid steric hindrance of functional tail groups or disorder. STM, the most used technique to characterize these mixed SAMs, inferred that phase separation exists; the subdomain compositions are very dependent on the chain lengths of each component and on the adsorption conditions (variation of temperature and concentration); Whitesides et al. described the co-adsorption of short- and long-chain alkanethiols on gold. They described the formation of microscopic subdomains and, for the first time, pointed out the fact that the composition of the SAM may not be that in solution.[16,17]

Note that mixed SAMs, often formed at room temperature, are most of the time not completely at equilibrium; phase-separated domains appear in which each component has the average structure of pure SAMs.[14,16] STM studies showed that phase segregation is strongly facilitated by different thiol chain lengths. Nevertheless, at 60 °C, exchanges with the solution were shown to favor single phase islands of one thiolate in the middle of a multiple domain phase.[17]

In this context, our objective was clearly to characterize and understand the behavior of mixed SAMs that contain a mixture of thiolates. Previous X-ray photoelectron spectroscopy (XPS) systematic study helped us to define conditions where the surface composition is very close to that in solution[18,19] and corresponding to complex, but rather homogeneous, atomic force microscopy (AFM) images.[19] This prompted us to use and combine other techniques to better characterize the layer structure of these SAMs at a molecular level.

Characterization of mixed SAM layers through a combination of experimental techniques and first principle calculations

* To whom correspondence should be addressed. E-mail: tielens@ccr.jussieu.fr.

10.1021/jp074023c CCC: $40.75
Published on Web 12/11/2007

enables to obtain fundamental insights on the organization of the thiol chains on a macroscopic level. Mixtures of different types of undecanethiol SAMs tend to organize in domains on the surface. Controlling the dispersion of SAM domains enables controlling of the dispersion of, e.g., biological systems to be attached on the SAM. The investigation of the substitution of the tail group (COOH/OH) will enable to shed some light on the dispersion mechanism within the mixed SAM but also on the chemistry at the border zones between the different domains.

In this work we study the adsorption of mercapto undecanethiol carboxylic acid (MUA) and mercapto undecanethiol alcohol (MUOH) from pure and 1:1 solutions on Au-nanostructured films. Adsorbed layers and interaction between tail groups will be characterized. In other words the geometry and the chemical properties of three different SAM systems are studied, using state of the art density functional theory (DFT) calculations, polarization modulation infrared reflection−absorption spectroscopy (PM-IRRAS), and XPS. The characterization of these undecanethiols is a logic continuation of our earlier works on the designing of biosensors.[18,19]

The results are presented as following: in the first part we discuss the PM-IRRAS results followed by XPS results on the three SAM systems, subsequently first principle results on the geometry relaxation, vibrational frequencies, and XPS results, are presented and confronted with the experimental results.

Experimental Details

1. Chemicals. 11-Mercaptoundecanoic acid (MUA) and 11-mercaptoundecanol (MUOH) were purchased from Sigma-Aldrich (Saint-Quentin Fallavier, France). All solvents were reagent grade. Reagents were used without any further purification. Experiments were carried out at room temperature.

2. Formation of Thiols SAMs. Glass substrates (11 mm × 11 mm) coated successively with a 50-Å thick layer of chromium and a 200-nm thick layer of gold were purchased from Arrandee (Werther, Germany). The gold-coated substrates were annealed by a brief passage in a flame to ensure a good crystallinity (flat (111) terraces) of the topmost layers, as recommended by the company, and rinsed in a bath of absolute ethanol during 15 min before adsorption. The substrates were immersed in freshly prepared pure solutions (MUA 100% and MUOH 100%) and binary mixture (MUA 50%−MUOH 50%) in absolute ethanol at a total thiol concentration of 10 mM for 3 h. After thorough rinsing in ethanol followed by ultrapure water rinsing and drying under a flow of dry nitrogen, the sample surfaces were analyzed in the air by PM-IRRAS and under vacuum by XPS.

3. PM-IRRAS Measurements. In the PM-IRRAS module, the sample is placed in the external beam of a Fourier transform infrared (FT-IR) instrument (Nicolet 5700 spectrometer), and reflected light is focused onto a nitrogen-cooled mercury cadmium telluride (MCT) detector at an optimal incident angle of 80−85°. A ZnSe grid polarizer and a ZnSe photoelastic modulator to modulate the incident beam between p and s polarizations (HINDS Instruments, PM90, modulation frequency = 36 kHz) are placed prior to the sample. The detector output is sent to a two-channel electronic device that generates the sum and difference interferograms. Those are processed and undergo Fourier transformation to produce the PM-IRRAS signal ($\Delta R/R^0$) = (Rp − Rs)/(Rp + Rs). All reported spectra are recorded at 8 cm^{-1} resolution by the co-addition of 128 scans; using a modulation of polarization enabled us to perform rapid analyses of the sample after immersion without purging the atmosphere or requiring a reference spectrum.

4. XPS Analysis. XPS analyses were performed on all samples using a PHOIBOS 100 X-ray photoelectron spectrometer from SPECS GmbH (Berlin, Germany) with the Mg Kα X-ray source ($h\nu$ = 1253.6 eV) operating at 10^{-10} Torr or less. Spectra were carried out with a 20-eV pass energy for the survey scan and 10-eV pass energy for the C1s, O1s, S2p, and Au4f regions. High-resolution XPS conditions have been fixed: "Fixed Analyzer Transmission" analyses mode, a 7 × 20 mm entrance slit, leading to a resolution of 0.1 eV for the spectrometer, and an electron beam power of 150 W (12.5 kV and 12 mA). Such a low energy is used in our experiments to keep the SAMs as intact as possible, to avoid possible defect when a high e-beam energy is applied to the sample. A takeoff angle of 90° from the surface was employed for each sample and binding energies were calibrated against the $Au4f_{7/2}$ binding energy at 84.0 eV. Element peak intensities were corrected by Scofield factors,[20] the spectra were fitted using the Casa XPS v.2.3.13 Software (Casa software Ltd. UK) and applying a Gaussian/Lorentzian ratio, G/L equal to 70/30. In addition, the error in the peak fitting process was estimated at 3% or less with respect to the integration of the raw data.

Computational Details

1. Methods. All calculations are performed using ab initio plane-wave pseudopotential periodic DFT as implemented in VASP.[20,21] The PBE functional[22−24] has been chosen to perform the periodic DFT calculations. The energy values are the most reliable that DFT can provide for evaluating the large aurophilic contribution that stabilizes the Au−Au bonds. The accuracy of the method has been tested elsewhere.[25−28] Only the valence electrons were treated explicitly and their interactions with the ionic cores are described by the projector augmented-wave method (PAW),[29,30] which allows the use of a low-energy cutoff (400 eV) for the plane-wave basis, with scalar relativistic effects included. Although the hydrogen bonding is very well described in DFT/PBE,[31] some caution should be taken concerning the dispersion forces between the CH_2 groups of the chains.

A 2 × 4 × 1 k-point grid is used in the Brillouin-zone sums, and the partial occupancies are set for each wave function using the tetrahedron method with Blöchl corrections.[32] The k-point choice emerges from a quality/cost ratio. The convergence was checked with the number of k-points for the Au(111) slab. It should be noted that the super cell counts about 90 atoms. The positions of all the atoms in the supercell are relaxed, keeping the bottom Au atoms fixed at their bulk positions, in the potential energy determined by the full quantum mechanical electronic structure until the total energy differences between the loops is less than 10^{-4} eV.

To calculate the Hessian matrix, finite differences are used, i.e., each ion is displaced in the direction of each Cartesian coordinate, and the Hessian matrix is determined from the forces. All atoms are displaced in all three Cartesian directions. The frequency calculations were performed considering one k-point.

To measure the binding energy (E) of core electrons using DFT calculations, two approximations can be made. In the "initial state approximation", it is assumed that the binding energy of the core electron is directly related to the energy level of its core orbital, $\epsilon_c(n_c)$, following Koopman's theorem.[33] In the "final state approximation", one must calculate the energy difference between two distinct states

$$\Delta E = E(n_c - 1) - E(n_c) \quad (1)$$

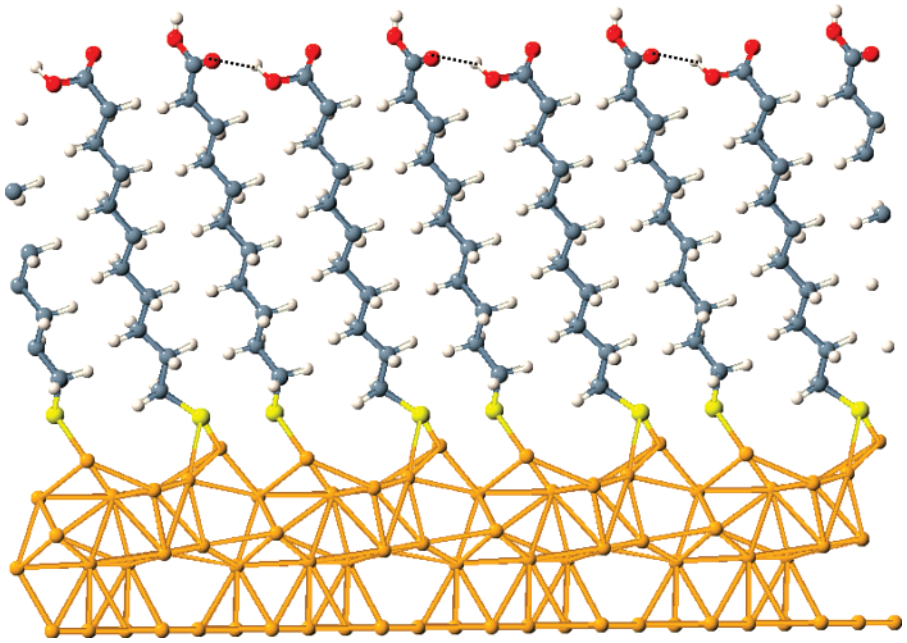

Figure 1. Periodic view of the optimized geometry for the MUA SAM, showing the H bond (dashed line) between two chains.

$E(n_c)$ is energy of the unexcited groundstate, and $E(n_c - 1)$ is the energy of the excited state where one electron is transferred from the core level of one particular atom (n_c) to the valence band. For such DFT calculations, we take advantage of the PAW formalism implemented in VASP because such an all-electron method with frozen core approximation also allows the generation of the corresponding core excited ionic potential during the calculations. Following the so-called "$(Z + 1)$ approximation", the core hole ($n_c - 1$) is modeled by adding one nuclear charge to the core atom and simultaneously one valence electron.[34] Hence, the screening by other valence electrons is included, whereas the screening by the core electrons is not taken into account. Actually, the difference given by eq 1 can be obtained using the Janak theorem[35]

$$\Delta E = E(n_c - 1) - E(n_c) \approx -\epsilon_c(n_c - {}^1/_2) \qquad (2)$$

$\epsilon_c(n_c - {}^1/_2)$ is the Kohn − Sham eigenvalue of the given core level with an occupation decreased by half an electron.

In the present study, both approaches (initial state and final state using the Janak theorem[35]) were used. The absolute values of the core level energy (initial state approximation) or of $\epsilon_c(n_c - {}^1/_2)$ (final state approximation) cannot be directly compared to experimental values (according to different reference energies in experiment and theory). As a consequence, only binding energy differences, ΔBE, for core states of the given atom in two different environments, are relevant for a comparison with data obtained from XPS analysis. For the ΔE (C 1s), we compared the values calculated for carbon atoms involved in different functions to that obtained for an aliphatic carbon in the chain (we observed that the C 1s binding energies of aliphatic carbons differ from each other by less than 0.03 eV). For the S 2p core level, we report the difference in the binding energy calculated for the nonequivalent S atoms obtained after optimization. The calculated value represents a mean value of S $2p_{3/2}$ and S $2p_{1/2}$ peak. Single-point calculations were performed using an increased cutoff energy (25%), without adding smearing, to reach a good accuracy of the calculation. The accuracy of the method of calculation was tested and we could reproduce experimental S 2p ΔE values from 0.2 to 0.6 eV.

All calculations were performed on an IBM regatta power4 of the supercomputing center IDRIS.

2. Description of the Model. It starts to be widely accepted that the thiolate SAM structure on Au(111) consists of an ordered $c(4 \times 2)$ super lattice containing 4 chains in both gas-phase and liquid environments.[6,36] In these lattices, the alkanthiolate molecules are chemisorbed on the Au surface by their S tails forming a thiolate bond, having tilt angles ranging from 20−40° with respect to the substrate normal.

The chemisorbed alkylthiolate chains adsorb as a $c(4 \times 2)$ pattern, being a little more stable than the $(\sqrt{3} \times \sqrt{3})R30°$ unit cell containing one chain. This supercell may have different combinations of orientated chains, making patterns all within an energy window of a few kcal/mol. This face is probably stabilized by the observed molecular pairing.

This study does not pretend to investigate all possible closed packed superstructures but the existing H-bond interactions between the different chains. Since the undecanethiol models have different relative geometries possible within a window of 1−2 kcal/mol, we have chosen to simulate the surface with a $(\sqrt{3} \times 2\sqrt{3})R30°$ unit cell. This choice emerges from a price/quality point of view. The surface layer was modeled by a minimal slab (3 hexagonal layers, as was used with success before in ref 37) with 6 atoms each. Two substituted undecanethiolate chains are adsorbed at one surface of the slab, and a vacuum of more than 12 Å (total z dimension being 35 Å) to avoid spurious interactions between neighboring replica (see Figure 1). In the past several studies have been undertaken in order to investigate the adsorption site of thiol chains on Au(111). The adsorption site is generally predicted using small models (one chain per unit cell) to be between the hollow and the bridge site (see ref 6 and references therein). This theoretical result is still under debate, since experimental results do not give a clear-cut answer (see the recent review of Vericat et al.[6]). Nevertheless, the initial adsorption site of our undecanthiol chains to start the geometry optimization was in the region of the hollow site on the Au(111) surface. Two initial geometries were tested in the first optimization cycles: the hollow and atop site. Finally we selected the most stable geometry to continue with: both chains positioned in the region of a hollow site. To

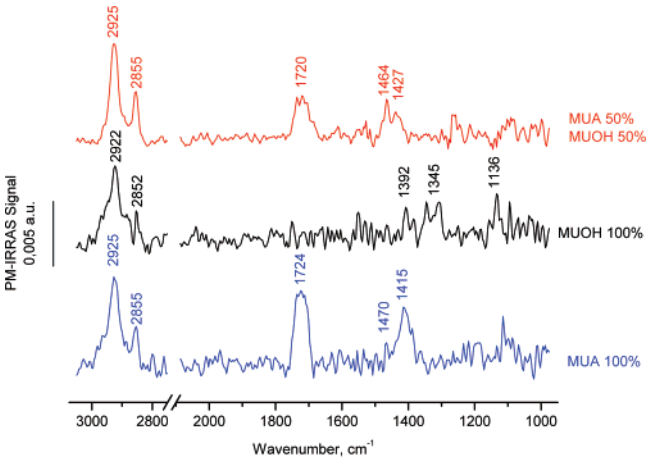

Figure 2. PM-IRRAS of MUA, MUOH, and MUA/MUOH 1:1 on gold surfaces.

find the geometry minimum on the potential surface the preconditioned residuum−minimization method was employed, which is expected to be the most reliable for large and complex systems.[38]

Results and Discussion

1. Surface Characterization of Thiol SAMs. *1.1. PM-IRRAS Results.* Figure 2 displays the PM-IRRA Spectra of the gold surface after immersion for 3 h in pure MUA, pure MUOH, and a 1:1 mixture of MUA and MUOH, rinsing in ethanol and ultrapure water and drying under dry N_2 flow. No band was ever observed at ~2550 cm^{-1}, the expected ν_{S-H} position, suggesting that all thiol molecules were anchored to the gold surface by formation of Au−S bonds. Two bands can be observed at 2925 and 2852 cm^{-1} on all three spectra, respectively assigned to the $\nu^{asym}_{CH_2}$ and the $\nu^{sym}_{CH_2}$ stretching modes of the alkyl groups[9] (see Table 1). The position of the asymmetrical contribution of the stretching mode at 2925 cm^{-1} is typical for a densely packed, though not perfectly crystalline, arrangement of the alkyl chain thiolates, where a perfectly crystalline phase would yield adsorption at around 2918 cm^{-1}.[13,19,39] Although, it is expected for pure thiolate layers to observe such a behavior, it is not straightforward for mixed layers. The fact that the $\nu^{asym}_{CH_2}$ contribution is observed at 2925 cm^{-1} for the three types of layers (see Figure 2) clearly suggests that the cristallinity of the mixed MUA-containing SAMs is not influenced by the substitution of the tail groups, in particular by possible interactions taking place between different terminal head groups.

In turning now to the 2000−1000 cm^{-1} region, the MUA spectrum exhibits two strong bands at 1725 and 1415 cm^{-1}, assigned respectively to the $\nu_{C=O}$ and $\nu_{C-O}/\nu^{sym}_{COO^-}$ stretching modes of the carboxylic/carboxylate groups. The former band is wider than usually observed,[9] which probably implies more than one contribution for the C═O stretching mode.[40] The spectrum associated with the pure layer of MUOH exhibits three weak contributions at 1392, 1345, and 1136 cm^{-1}, assigned to δ_{OH} for the two former bands and to ν_{C-O} stretching mode for the latter one. For the mixed MUA/MUOH SAM, one can notice, first, a decrease by half of the intensity of the 1720-cm^{-1} band along with the presence of bands present in both pure SAM spectra and, second, a small increase of the $\nu_{C=O}$ bandwidth. These two points clearly suggest the presence of a mixed layer of both kinds of alkyl thiolate chains; however the broadening of the C═O stretching band suggests that the C═O bonds are affected by several types of interaction. The latter point will be discussed here below.

1.2. XPS Results. Figure 3 and Table 2, which show and describe the C 1s peak of the three studied surfaces, provide evidence that thiolates are adsorbed in a very similar total amount. Moreover the decomposition of each C 1s peak into two or three contributions gives additional information concerning the fraction of each thiol in the layers.

On the pure MUOH layer, the C 1s peak could be decomposed into two contributions, at 284.9 and 286.6 eV, respectively. The one at 284.9 eV is obviously due to the carbon atoms of the aliphatic chain, while that at higher BE is attributed to the carbon in the COH tail groups. On the MUA layer, two contributions, in addition to the one of the aliphatic carbons, were necessary to fit the peak, one at 289.2 eV clearly attributed to the carbon in COOH groups while that at 286.2 eV may be ascribed to the carbon in α position of either the sulfur atom or the COOH terminal group in agreement with previous investigations;[9] the latter hypothesis is more likely since the carbon adjacent to the sulfur atom is deeply buried in the layer and probably hardly detected.[9]

Eventually, on the mixed MUOH/MUA layer, the C 1s peak was best fit with four contributions consistent with the fact that both MUA and MUOH are present on the surface. Noticeable are the areas of the various contributions that suggest very close amounts of carbon atoms in COOH and COH groups, i.e., very similar concentrations of each thiol in the adsorbed phase.

Complementary information is brought by analyzing the sulfur XPS peaks on each layer. Figure 4 and Table 3 show the S 2p peaks and associated BE, corresponding to the pure MUA, MUOH, and MUA50/MUOH50 layers, respectively. Each of these signals was best fit with two doublets, referred as S1 and S2 in Table 3, identical binding energies on the three surfaces. These doublets are the S $2p_{1/2}$ and $2p_{3/2}$ contributions, with the normal 2:1 area ratio and 1.2-eV splitting; the S $2p_{3/2}$ peaks are located at 161.9 ± 0.1 and 162.4 ± 0.1 eV; the former BE value is that expected for S−Au bonds in thiolate species;[9,41] the second doublet, located ca. 0.5 eV upward can hardly be attributed to unbound sulfur (too low BE).[42,43] The presence of a second doublet, only shifted by 0.4−0.5 eV, rather suggests the existence of two different binding sites; this is still a topic of discussion in recent papers.[42,44,45] This possible interpretation will be discussed in the light of theoretical data presented here

TABLE 1: Theoretical and Experimental Vibrational Frequencies for the Three SAMs (Values in cm^{-1})

	ν_{OH}	$\nu^{asym}_{CH_2}$	$\nu^{sym}_{CH_2}$	ν_{C-O}	$\delta^{sym}_{CH_2}$	$\nu^{sym}_{COO^-}/\nu^{acid}_{C-O}$	δ^{alc}_{OH}	ν^{alc}_{C-O}
MUA exp		2925	2855	1724	1470	1415		
MUA theo	3624	3074−30 13		1717				
	3437			1743				
MUOH exp		2922	2852				1392	1136
							1345	
MUOH theo	3642	3074−30 17						
	3611							
Mixed 1:1 exp		2925	2855	1720	1464	1427		1109
Mixed 1:1 theo	3655	3074−30 13		1724				
	3645							

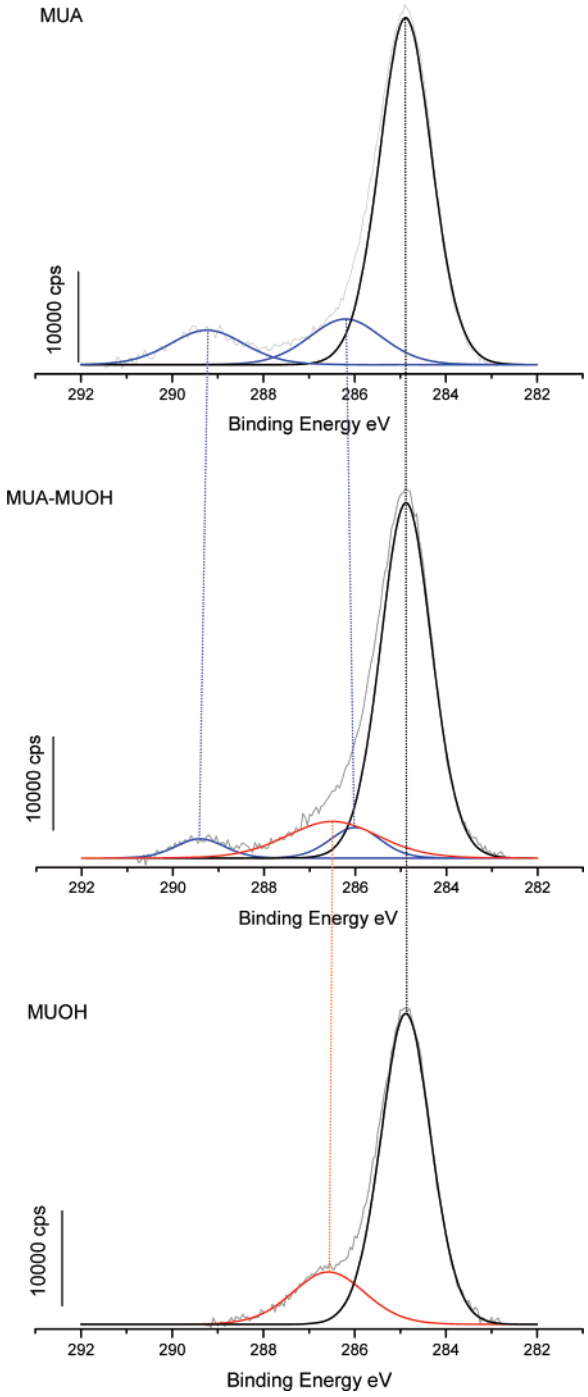

Figure 3. XPS C 1s region for the different SAMs considered.

below. Note here again that the three S 2p peak areas are very similar, confirming very close values of the coverage of the three different SAMs.

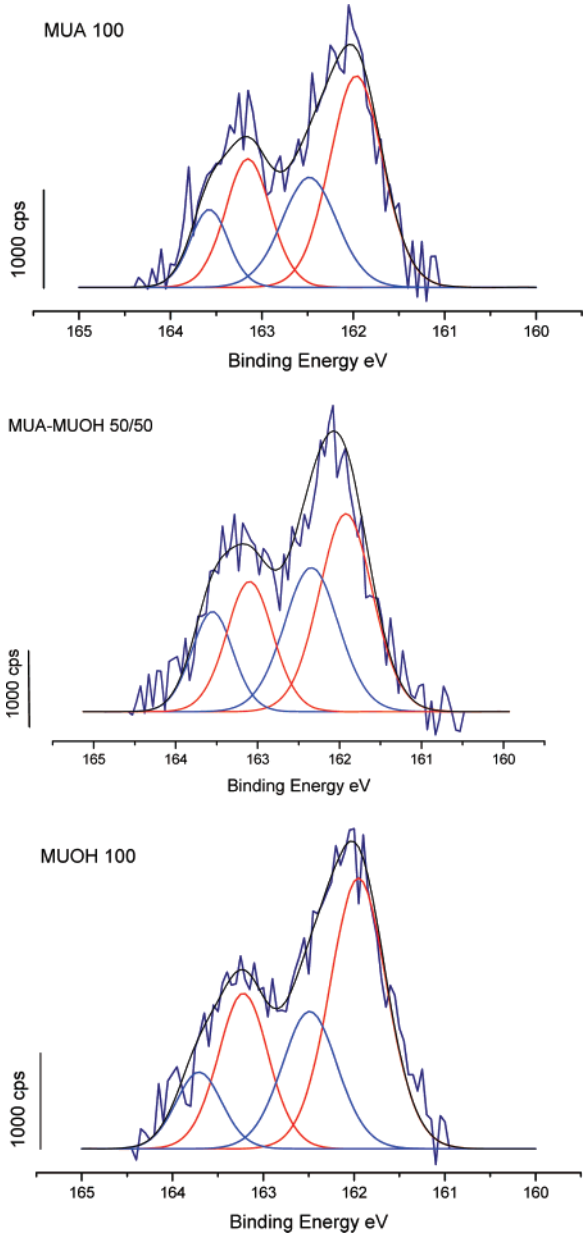

Figure 4. XPS S 2p region for the different SAMs considered.

The O 1s peaks were also recorded (see Figure 5 and Table 4). The MUA layer spectrum is made of two main contributions at 532.1 and 533.1 ± 0.2 eV respectively; the former is at a binding energy close to that of oxygen in C═O or COO^- groups; the second contribution is likely due to oxygen in the acidic OH group; note that similar O 1s BEs were found by other authors in the spectrum of carboxylic-terminated thiols on gold;[46,47] an additional contribution at 534 ± 0.2 eV was necessary to fit the peak, attributed to oxygen in residual water.

TABLE 2: Measured (XPS) and Calculated (VASP, Initial State Approximation) C 1s Core Level Shifts ΔBE for the Different SAMs Considered (Experimental Accuracy Is 0.1 eV)

		(HO)−*C*═O	−**C**−OH	−*C*−S	−*C*−(COOH)	*C*−C, *C*−H
MUA	eV	289.2			286.2	284.9
	Δ*E* (measured)	4.3			1.3	0
	Δ*E* (calcd)	3.3		0.9	0.3	0
MUOH	eV		286.6			284.9
	Δ*E* (measured)		1.7			0
	Δ*E* (calcd)		1.3	0.9		0
mixed 1:1	eV	289.2	286.8		286.0	284.9
	Δ*E* (measured)	4.5	1.6		1.1	0
	Δ*E* (calcd)	3.6	0.6	0.7	0.3	0

TABLE 3: Measured (XPS) and Calculated (VASP, Initial State Approximation) S 2p Core Levels for the Different SAMs Considered (S1 and S2 Refer to the Two Different Observed Chemical States of S, the Experimental Accuracy Is 0.1 eV, for the S 2p Peak, the Fitting Was Performed Conserving the 3/2/1/2 Ratio of Two, with a Deviation of Approximately 10%)

	eV	S $2p_{3/2}$	S $2p_{1/2}$	ΔE (S1−S2) measured	ΔE_{calc}
MUA	S1	162.0	163.1	0.5	0.43
	S2	162.5	163.6		
MUOH	S1	161.9	163.2	0.6	0.35
	S2	162.5	163.7		
mixed 1:1	S1	161.9	163.1	0.5	0.50
	S2	162.4	163.6		

As for the MUOH layer, the main peak at 533.0 ± 0.2 eV, may be attributed to oxygen of the OH tail group; this attribution seems a little bit high, however already observed for OH-terminated alkanethiols on gold.[13] Eventually, the spectrum of the mixed MUOH/MUA layer is dominated by an intense contribution at 533.1 ± 0.2 eV, corresponding to oxygens in OH groups of the MUA or MUOH tail groups, and a smaller one at 532.1 ± 0.2 eV attributed to the C═O oxygens; a peak at 534 ± 0.2 eV is again present confirming the presence of a small amount of water within the layer.

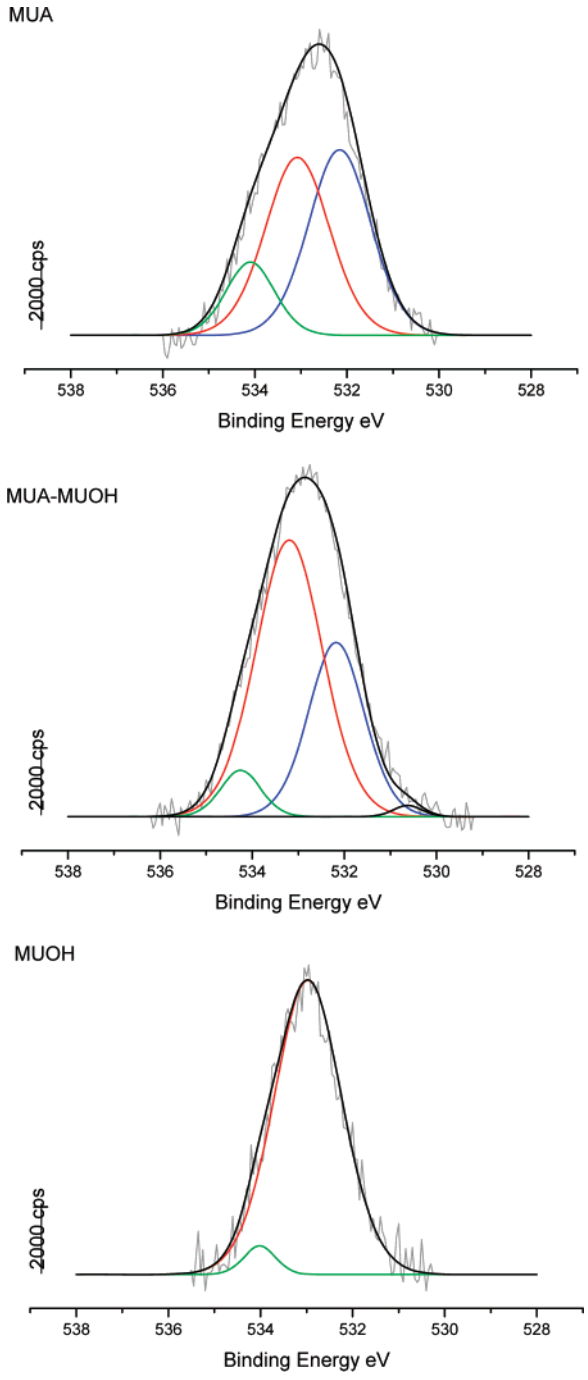

Figure 5. XPS O 1s region for the different SAMs considered.

TABLE 4: XPS O 1s BE (*E*) Results for the Different SAMs Considered (Vaues in eV, Experimental Accuracy Is 0.1 eV)

	(HO)−C═*O*	−C−*O*−H	O═C−*O*−H	H_2O
MUA	532.1		533.1	534.2
MUOH		533.0		534.0
mixed 1:1	532.1	533.1		534.2

As a summary, the XPS results constitute a set of data that suggests MUA, MUOH, or an almost equimolecular mixture of MUA + MUOH thiolates. All these thiols are bound to gold, and an important data is the observation of two different types of S bonds that may be attributed to two different adsorption sites. This requires additional discussion after theoretical considerations.

2. Theoretical Results. *2.1. Geometry of the Thiol SAMs.* In this section we summarize the results obtained for the geometry optimization of the gold surface, the sulfur anchoring, the chains, and the tail group geometry after full relaxation of the three different systems considered (the MUA, MUOH, and 1:1 mixture).

One can immediately note (see Figure 1) that the gold slab is greatly affected upon thiol adsorption. This phenomenon might be slightly accentuated in comparison with former studies using smaller super cells, due to the use of a relative large unit cell, which allows more important relaxation effects, but also the fact that only 3 layers of bulk were considered. Nevertheless, the magnitude of the corrugation is in line with the fact that the Au(111) surface easily reconstructs, certainly in comparison with other coinage metals.[48,49] This might also be the reason why it is not always straightforward to assign the adsorption site experimentally.

The sulfur atoms bound to the Au(111) surface are found close to the bridge positions and close to the on top positions. The two adsorption sites have sulfur−gold bond lengths of 2.48 and 2.36 Å, respectively. These bond lengths are similar to ∼2.5 Å, found in earlier studies.[50,51] Depending on the used techniques, the energetically most favorable binding site found experimentally is the hollow,[52,53] the bridge,[54] or the half-bridge (shifted on top)[55] site. Most theoretical simulations predict a close to bridge position in the case of pure alkanethiolates,[50,51,56] although on top position is found as well.[57] It is interesting to note that no consensus on this point has been reached. The optimized geometry shows two different bending angles of sulfur, $\theta_{(C-S-Au)}$ = 112.9 and 117.6° for the bridge site and 117.0° for the almost atop site, i.e., confirming the stability of unit cells larger that the $(\sqrt{3} \times \sqrt{3})R30°$ one. It is suspected that the deviation of the second angles from the equilibrium sp^3 hybridization (104.5°) is caused by the twist produced by the intermolecular repulsion, i.e., showing an almost sp^2 hybridization. In other models,[51,58] similar $\theta_{(C-S-Au)}$ angles are found for pure alkanethiolates. This result shows that the substitution of the tail group has no important effect on the S chemisorption geometry for this length of alkane chains, and confirms the flexibility of the AuS bond, as well as the possibility of having different adsorption geometries for the chain within a small energy range. This result can explain why two different sulfur doublets are observed in the XPS spectra. Indeed, the two peaks can be attributed to two different

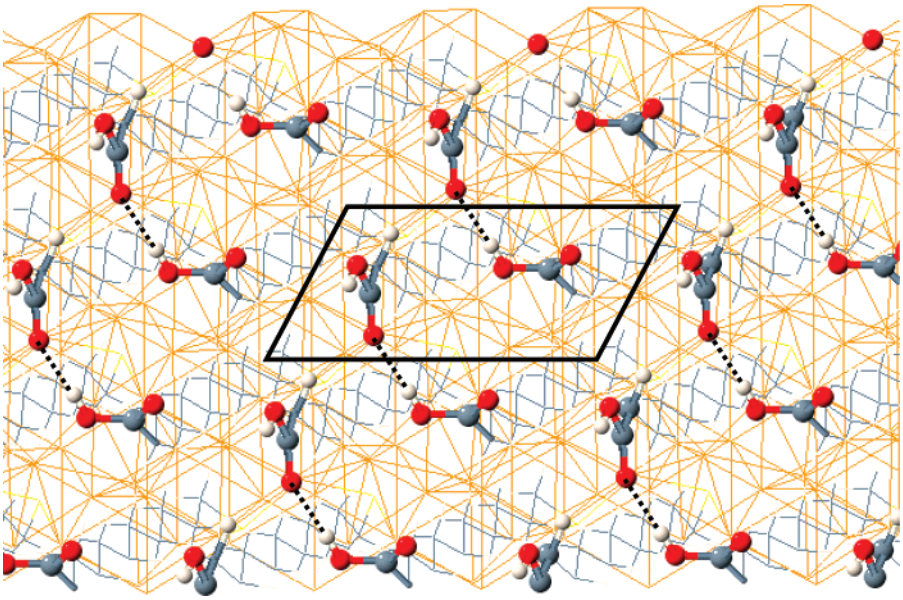

Figure 6. Tail groups seen from above the MUA SAM showing the H-bond. (Red, oxygen; white, hydrogen; gray, carbon; yellow, surfur; orange, gold). $(\sqrt{3} \times 2\sqrt{3})$R30° unit cell depicted in black.

adsorption sites; one close to the on top site and another one almost bridge site. Looking at the relative intensities and on the basis of recent STM[45] and other theoretical results,[50,51,56] one suggests the following: the relative intensity for both S doublets is 1−2, meaning a unit cell containing three thiol chains. However, vide infra, it is supposed that the chains organize as coexisting $(\sqrt{3} \times \sqrt{3})R30°$ unit cells containing one thiol chain and $c(4 \times 2)$ unit cells containing 4 chains. The average signal of such a complex pattern could explain the observed 1−2 intensity ratio. It should be noted that after substitution of the tail group, the sulfur−gold bonding geometry remains the same. The characteristic angles, almost, do not change. The tail group orientations are the most affected by the substitution.

The geometry of alkanthiolate chains is characterized by the tilt θ, the rotation φ (φ = dihedral between NNN Au atoms and S−C_1), and the twist χ angles (χ = dihedral between S−C_1 and C_{10}−C_{11}). The tilt angle is for both chains equal to ($\theta \approx 30°$) and similar to the pure alkanthiolate chains.[45] That of the rotation is fairly also in agreement with nonsubstituted chains, yielding $\varphi = +23°$ for the bridge site and $-17°$ for the atop site. The twist angle $\chi = 136.9°$ for the bridge and $-16°$ for the atop conformation, the twist angle for the bridge conformation is in agreement with the most stable conformation proposed by Riposan et al.[45] via STM analysis.

In the case of the MUA SAM, the formation of one hydrogen bond between COOH tail groups is observed (see Figure 6). The distance between the carbonyl oxygen atom of one chain and the hydroxyl hydrogen of the neighboring chain is found to be 1.933 Å. One can imagine several such short distances between the carbonyl groups and the hydroxyl groups of neighboring chains; however in the present case only one H bond is found between the chains, probably, because of sterical hindering of the voluminous carboxyl groups. After substitution of one carboxyl tail group by a hydroxyl tail group the H-bond interaction is preserved; the C═O···H−O distance decreases to 1.885 Å. In the case of the pure alcohol thiolate SAMs (MUOH) the interaction between the chains increases, until a distance of 1.969 Å for the intermolecular H-bond is reached.

2.2. Vibrational Frequency Analysis. The vibrational frequencies of the SAM structures were calculated (more than 240) first to check if the optimized geometry was indeed an energy minimum on the potential energy surface. No imaginary frequencies were found, which confirms that our model is a minimal energy structure. In a second stage the most interesting frequencies were compared with the experimental ones (see Table 1).

Only the most representative frequencies (see Table 1) were selected to be compared with the experimental PM-IRRAS spectrum (due to technical limitation only vibrations up to 2500 cm^{-1} could be measured). The selection was made on the basis of there vibration vectors and associated selection rules. Finally three characteristic vibrational domains were considered in order to characterize the SAMs: the ν_{OH}, $\nu_{CH_2}^{asym}$, and the ν_{C-O}.

The frequency region 3800−3300 cm^{-1} is typically associated with the ν_{OH} stretching modes, the highest frequencies being assigned to non-hydrogen-bonded hydroxyl groups. In our calculations this absorption range consists of two frequencies, since only two hydroxyl groups are present in our model.

The unperturbed hydroxyl group of the carboxyl tail group, which is present in MUA and mixed 1:1 SAMs, is found to have a vibrational frequency between 3655 and 3624 cm^{-1}. The unperturbed hydroxyl group of the alcohol tail group, present in the MUOH, has a vibrational frequency of 3642 cm^{-1}. The least perturbed OH group is found in the alcohol group of the mixed 1:1 SAM (3645 cm^{-1}), and the most perturbed OH group, implicated in the strongest H-bond, is found in the MUA SAM (3437 cm^{-1}, which is a decrease of 200 cm^{-1}, with respect to the unperturbed one). The perturbed OH group of the MUOH SAM has vibrational frequency of 3611 cm^{-1}.

One group is involved in an H bond while the other is almost unperturbed. The largest shift is found in the case of the pure MUA SAM. The theoretical calculated frequencies are in very good agreement with experimental finding of Bain et al.[9] who observed this phenomenon. Quantitatively, however we notice the well-known overestimation of DFT methods for such type of vibrations.[59] We deliberately did not correct the frequencies with a scaling factor since in our case we should have needed at least two scaling factors, one for the OH vibrations and one for the CH vibrations. The latter is also known to be overestimated but with a different magnitude. So, being aware of the limitations of the calculation technique we preferred to present

the raw data. From the combination of the geometry optimization results and the vibrational frequencies one can predict the existence of only one interaction between two chains.

The second group of bands is assigned to the CH vibrations. These bands, as already mentioned above, are used as a measure of the so-called crystallinity or trans-gauche ratio in the chain conformations. At the chain length used ($n = 11$) the polymethylene chain is expected to be relatively ordered; i.e., in an all-trans conformation. From the theoretical frequencies calculated for the three SAMs, one can deduce that the crystallinity is not affected by the substitution of the tail group, which is in agreement with the experimental IR data. The band between 3100−3000 cm^{-1} is present in the three systems, however, also overestimated in comparison with the experimental values.

The next band around 1725 cm^{-1} is the finger print of the carbonyl group. These frequencies are very well reproduced in our model calculations; from a quantitatively and a quantitatively point of view. Indeed, for the MUA spectrum two frequencies are observed, one at 1717 cm^{-1} and a second at 1743 cm^{-1}. The presence of two different carbonyl groups is in line with the existence of only one H bond between the hydroxyl and carbonyl groups of chain tails (see Figure 6). This result can also explain the broadening of the experimentally observed band around 1725 cm^{-1}. In the case of the mixed 1:1 SAM only one vibration is found, 1724 cm^{-1}, since only one carbonyl group is inferred by the model (vide supra). It should be noted that, in a mixture, band broadening is observed when more than one type of carbonyl vibration is found theoretically, which is caused by carbonyls involved in more than one type of interaction. In our experimental spectrum such a band broadening is noticed, which can be explained as follows: in a microscopically perfect mixture (every MUA having only MUOH neighbors; i.e., without aggregation), all carbonyl groups of the MUA chains are implicated in the H-bond with a hydroxyl group of a MUOH chain. This should be seen in the IR spectra by a sharp band assigned to the only type of carbonyl present. However, when the mixture is not completely perfect and the carbonyl group of the MUA chain is in interaction with another MUA chain, two extra bands show up. Indeed, one for the carbonyl group H bonded with another carbonyl of a neighboring MUA chain and another bands assigned to non-H-bonded carbonyl (similar to the case in a pure MUA SAM). The appearance of these two extra bands in a theoretical spectrum has a band broadening effect. In our experimental spectrum for the 1:1 mixture such a band broadening is observed, suggesting the formation of aggregated pure MUA and pure MUOH coexisting with a perfect mixture. Looking at the band shape, the most intense band is the one associated to the 1:1 mixture.

In summary, the experimental and theoretical vibrational specta clearly show finger prints of an interaction between tail groups. Moreover one can deduce the existence of only one type of interaction prevailing between the chains, and that only some traces of aggregation of the MUA and MUOH chains are present, as was concluded in our former study, showing rather homogeneous AFM images.[18]

2.3. Electronic Core Level Calculations. The consistency of the mixed experimental−theoretical approach in comparing the calculated core levels with the experimental ones for the C 1s and S 2p core electrons was investigated (see Tables 2 and 3). For the C 1s core level, the main observed tendency in the binding energy: *C*H < *C*−COOH < *C*−OH < O*C*OH is reproduced by the theoretical calculations. The binding energy shift is lower than the experimental one. This shows that the XPS shifts for carbon, in the different environments, are at least partly related to initial states effects (i.e., shifts of the electronic levels and/or electron transfer in the fundamental state). Unfortunately, any attempt to take into account final state effects (within the ($Z + 1$ or the Janak's approximation[34]) failed to enhance the accuracy of the results. This defect of the method was foreseen in the early 80s and is due to the inadequacy of the ($Z + 1$) approximation in the case of some carbon containing molecules as CO.[60] A C−S binding energy of 1 eV higher than the C−H one was calculated. As already stated in the experimental part, due to the length of the SAM chain, the carbon atoms in C−S may be attenuated by the SAM and their contribution may not be measurable by XPS.

With regards to the S 2p core levels, initial and final state calculations led to similar tendencies: Indeed, a difference in binding energy between both types of S atoms of ∼0.4 eV was calculated at the initial state. The bridging S atom (S2) is 0.4 eV higher in energy than the atop S, in agreement with an increase of the binding energy with the coordination number; this result is conserved at the final state, where a higher binding energy of 0.6 eV is calculated for the bridging sulfur atom. To summarize, reasonably good agreement between theory and experience concerning the XPS results is found, justifying the choice of our model, which is an important point. The two different binding energies for the S atoms, confirm different adsorption sites of the thiol chain with the Au(111) surface.

Conclusions

In this study, we have characterized the structure of undecanethiol SAMs on Au(111) with −COOH and −OH tail groups. The pure and mixed SAMs were investigated. We showed evidence that the thiol chains are adsorbed on different types of sites on the surface and that the tail groups interact with each other via one H bond, resulting into chain pairing. The composition of the SAM mixture was found to be close to the concentration in solution, and more importantly, some segregation and formation of pure (MUA and MUOH) domains was inferred from the combination of theoretical and experimental results.

A very good agreement is found between experimental and theoretical vibration analyses. The CH vibrations (experimental and theoretical) suggest that the crystallinity of the SAM does not change upon tail group substitution. The interaction taking place between the different tail groups has no influence on the order of the alkyl chains. The carbonyl vibrational frequencies clearly suggest the presence of H bond between chains. The theoretical results for the OH stretching frequencies are an extra indication of the weakening of the OH bond due to the formation of a H bond with a neighboring chain.

XPS results confirmed that on the mixed MUA/MUOH layer both components are equally represented. Moreover, the presence of two different types of sulfur was associated to different adsorption sites of the thiol chains. This result confirms the suggestion that the thiol chains adsorb as patterns having unit cells which are larger than the simple ($\sqrt{3} \times \sqrt{3}$)*R*30°. This result was also found in our DFT calculations for the fully relaxed model (top layers of the slab and the SAM).

The ab initio calculations suggest the formation of a single H bond between the tail groups of the thiol chains. Interchain distances between the tail groups are found around 1.9 Å, which are in the range of a H bond. H bonds are found in the pure as in the mixed cases.

It was also concluded using PM-IRRAS measurements and ab initio calculations that our preparation method for the mixed substituted undecanethiol chains show some traces of segrega-

tion (formation of pure MUA and pure MUOH domains within on the mixed SAM Surface). This inhomogeneity on the SAM surface will have certainly an effect on the reactivity of the whole modified surface and is planned to be investigated with the tools provided by DFT reactivity theory.

We have shown that mixed undecane thiol SAMs can be prepared as highly ordered systems, which would improve the specific adsorption properties of the SAMs, especially, in the field of organic-on-organic growth and the dispersion of biological systems.

Acknowledgment. The authors thank IDRIS and CCRE (Université Pierrre et Marie Curie) for providing the computation facilities.

References and Notes

(1) Poirier, G. *Chem. Rev.* **1997**, *97*, 1117.
(2) Ulman, A. *Chem. Rev.* **1996**, *96*, 1533.
(3) Porter, M. D.; Bright, T. B.; Allara, D. L.; Chidsey, C. E. D. *J. Am. Chem. Soc.* **1987**, *109*, 3559.
(4) Dubois, L. H.; Nuzzo, R. G. *Annu. Rev. Phys. Chem.* **1992**, *43*, 437.
(5) Love, J. C.; Estroff, L. A.; Kriebel, J. K.; Nuzzo, R. G.; Whitesides, G. M. *Chem. Rev.* **2005**, *105*, 1103.
(6) Vericat, C.; Vela, M. E.; Benitez, G. A.; Matin, Gago, J. A.; Torrelles, X.; Salvarezza, R. C. *J. Phys.: Condens. Matter* **2006**, *18*, R867.
(7) Houssiau, L.; Bertrand, P. *Appl. Surf. Sci.* **2001**, *175*−*176*, 399.
(8) Truong, K. D.; Rowntree, P. A. *Prog. Surf. Sci.* **1995**, *50*, 207.
(9) Bain, C. D.; Troughton, E. B.; Tao, Y.-T.; Evall, J.; Whitesides, G. M.; Nuzzo, R. G. *J. Am. Chem. Soc.* **1989**, *111*, 321.
(10) Schreiber, F. *Prog. Surf. Sci.* **2000**, *65*, 151.
(11) Wadu-Mesthrige, K.; Amro, N. A. *Scanning* **2000**, *22*, 380.
(12) Patel, N.; D. M. C.; Hartshorne, M.; Heaton, R. J.; Roberts, C. J.; Tendler, S. J. B.; Williams, P. M. *Langmuir* **1997**, *13*, 6485.
(13) Nuzzo, R. G.; Dubois, L. H.; Allara, D. L. *J. Am. Chem. Soc.* **1990**, *112*, 558.
(14) Sawaguchi, T.; Sato, Y.; Mizutani, F. *J. Electroanal. Chem.* **2001**, *496*, 50.
(15) Methivier, C.; Beccard, B.; Pradier, C.-M. *Langmuir* **2003**, *19*, 8807.
(16) Folkers, J. P.; Laibinis, P. E.; Whitesides, G. M. *Langmuir* **1992**, *8*, 1330.
(17) Folkers, J. P.; Laibinis, P. E.; Whitesides, G. M. *J. Phys. Chem.* **1994**, *98*, 563.
(18) Briand, E.; Salmain, M.; Compère, C.; Pradier, C. M. *Colloids Surf. B: Biointerf.* **2006**, *53*, 215.
(19) Briand, E.; Salmain, M.; Herry, J. M.; Perrot, H.; Compère, C.; Pradier, C. M. *Biosens. Bioelectron.* **2006**, *22*, 440.
(20) Kresse, G.; Hafner, J. *Phys. Rev. B* **1994**, *49*, 14251.
(21) Kresse, G.; Furthmuller, J. *Comput. Mater. Sci.* **1996**, *6*, 15.
(22) Perdew, J. P.; Burke, K.; Ernzerhof, M. *Phys. Rev. Lett.* **1996**, *77*, 3865.
(23) Perdew, J. P.; Burke, K.; Ernzerhof, M. *Phys. Rev. Lett.* **1997**, *78*, 1396.
(24) Zhang, Y. K.; Yang, W. T. *Phys. Rev. Lett.* **1998**, *80*, 890.
(25) Gu, X.; Ji, M.; Wei, S. H.; Gong, X. G. *Phys. Rev. B* **2004**, *70*, 205401.
(26) Tielens, F.; Andrés, J.; Van Brussel, M.; Buess-Herman, C.; Geerlings, P. *J. Phys. Chem. B* **2005**, *109*, 7624.
(27) Visart de Bocarmé, T.; Chau, T.-D.; Tielens, F.; Andrés, J.; Gaspar, P.; Wang, R. L. C.; Kreuzer, H. J.; Kruse, N. *J. Chem. Phys.* **2006**, *125*, 1.
(28) Tielens, F.; Andrés, J. *J. Phys. Chem. C* **2007**, *111*, 10342.
(29) Blöchl, P. E. *Phys. Rev. B* **1994**, *50*, 17953.
(30) Kresse, G.; Joubert, J. *Phys. Rev. B* **1999**, *59*, 1758.
(31) Adamo, C.; Barone, V. *J. Chem. Phys.* **1999**, *110*, 6158.
(32) Blöchl, P. E.; Jepsen, O.; Andersen, O. K. *Phys. Rev. B* **1994**, *49*, 16223.
(33) Koopmans, T. *Physica* **1933**, *1*, 104.
(34) Johansson, B.; Mårtensson, N. *Phys. Rev. B* **1980**, *21*, 4427.
(35) Janak, J. F. *Phys. Rev. B* **1978**, *18*, 7165.
(36) Schreiber, F. *J. Phys.: Condens. Matter* **2004**, *16*, R881.
(37) Franzen, S. *Chem. Phys. Lett.* **2003**, *381*, 315.
(38) VASP. Manual http://cms.mpi.univie.ac.at/vasp/.
(39) Bertilsson, L.; Liedberg, B. *Langmuir* **1993**, *9*, 141.
(40) Lestelius, M.; Liedberg, B.; Tengvall, P. *Langmuir* **1997**, *13*, 5900.
(41) Wirde, M.; Gelius, U.; Nyholm, L. *Langmuir* **1999**, *15*, 6370.
(42) Castner, D. G.; Hinds, K.; Granger, D. W. *Langmuir* **1996**, *12*, 5083.
(43) Nuzzo, R. G.; Dubois, L. H.; Allara, D. L. *J. Am. Chem. Soc.* **1987**, *109*, 733.
(44) Walczak, M. M.; Alves, C. A.; Lamp, B. D.; Porter, M. D. *J. Electroanal. Chem.* **1995**, *396*, 103.
(45) Riposan, A.; Liu, G. Y. *J. Phys. Chem. B* **2006**, *110*, 23926.
(46) Yang, C. H.; Dermody, D. L.; Xu, C.; Ricco, A. J.; Crooks, R. M. *Langmuir* **1996**, *12*, 726.
(47) Yang, Z. P.; Engquist, I.; Wirde, M.; Kauffmann, J. M.; Gelius, U.; Liedberg, B. *Langmuir* **1997**, *13*, 3210.
(48) Crljen, Z.; Lazic, P.; Sokcevic, D.; Brako, R. *Phys. Rev. B* **2003**, *68*, 195411.
(49) Galanakis, I.; Papanikolau, N.; Dederichs, P. H. *Surf. Sci.* **2002**, *511*, 1.
(50) Fischer, D.; Curioni, A.; Andreoni, W. *Langmuir* **2003**, *19*, 3567.
(51) De Renzi, V.; Di Felice, R.; Marchetto, D.; Biagi, R.; del Pennino, U.; Selloni, A. *J. Phys. Chem. B* **2005**, *108*, 16.
(52) Zang, L.; Goddard, W. A., III; Jiang, S. *J. Chem. Phys.* **2002**, *117*, 7342.
(53) Tachibana, M.; Yoshizawa, K.; Gawa, A.; Fujimoto, H.; Hoffman, R. *J. Phys. Chem. B* **2002**, *106*, 12727.
(54) Vargas, M. C.; Giannozzi, P.; Selloni, A.; Scoles, G. *J. Phys. Chem. B* **2001**, *105*, 9509.
(55) Morikawa, Y.; Liew, C. C.; Nozoye, H. *Surf. Sci.* **2002**, *514*, 389.
(56) Maksymovych, P.; Sorescu, D. C.; Yates, J. T., Jr. *J. Phys. Chem. B* **2006**, *110*, 21161.
(57) Cao, Y.; Ge, Q.; Dyer, D. J.; Wang, L. *J. Phys. Chem. B* **2003**, *107*, 3803.
(58) Li, T.-W.; Tao, Y.-T. *J. Phys. Chem. B* **1998**, *102*, 2935.
(59) Johansson, M. P.; Sundholm, D.; Vaara, J. *Angew. Chem., Int. Ed.* **2004**, *43*, 2678.
(60) Tomanek, D.; Dowben, P. A.; Grunze, M. *Surf. Sci.* **1983**, *126*, 112.